Journal of the Physical Society of Japan
Vol. 71, No. 7, July, 2002, pp. 1732–1739

Magnetoelastic Effect in Holmium Studied by X-Ray Diffraction

Hiroyuki OHSUMI*

Department of Physics, Faculty of Science and Technology,
Keio University, Hiyoshi, Yokohama 223-8522

(Received January 23, 2001)

X-ray diffraction measurements have been performed on a single crystal sample of the rare earth metal holmium. The temperature and magnetic field dependence of the *c*-lattice parameter was studied in detail below the Néel temperature of 132 K. Magnetic structural phase transitions were observed as a change in the *c*-lattice parameter. In addition, lattice modulations induced by the magnetic structure were investigated by observing satellite reflections. A model based on the exchange magnetostriction can explain these magnetostrictive behaviors. The magnetic structures which were used in the analysis were reproduced by the self-consistent mean field calculation. The model has explained the temperature and magnetic field dependence of the *c*-lattice parameter, as well as the behaviors of the wave number and the amplitude of the lattice modulation.

KEYWORDS: holmium, helifan, magnetoelastic effect, lattice modulation, X-ray diffraction
DOI: 10.1143/JPSJ.71.1732

1. Introduction

In this paper, we describe the detailed results of X-ray diffraction experiments on the rare earth metal holmium.[1,2] Our main purpose on this work is to elucidate the influence of a magnetic structure on a crystal lattice. Specifically, a microscopic magnetoelastic effect, which appears as a lattice modulation, has been investigated precisely. Holmium shows various magnetic structures, which is a great advantage in analyzing the effect of a magnetic structure on a crystal lattice. In this regard, holmium is considered to be a suitable system for studying the magnetoelastic effect. Further, the magnetic structures of holmium are well established by earlier studies.[3–12]

Metallic holmium exhibits a helical magnetic structure[3–11] in a temperature range between the Néel temperature of 132 K and the Curie temperature of 20 K. Various magnetic structural changes are induced by application of a magnetic field in the hexagonal *c*-plane.[4,12] Magnetization process of the helical magnetic structure was explained by Kitano and Nagamiya.[13] The helix structure is first distorted so as to induce magnetization, and then undergoes a first-order transition to a fan structure in which the magnetic moments oscillate around the field direction. An increase of the magnetic field reduces continuously the amplitude of the oscillation and finally a ferromagnetic structure appears with a second-order transition. Results of various experiments on holmium[4,14,15] suggested the existence of an extra new phase. Figure 1(a) shows the schematic *H–T* phase diagram[4] of holmium for the magnetic field along the *b*-axis. The extra phase corresponds to the phase I in this figure and its magnetic structure had remained undetermined for

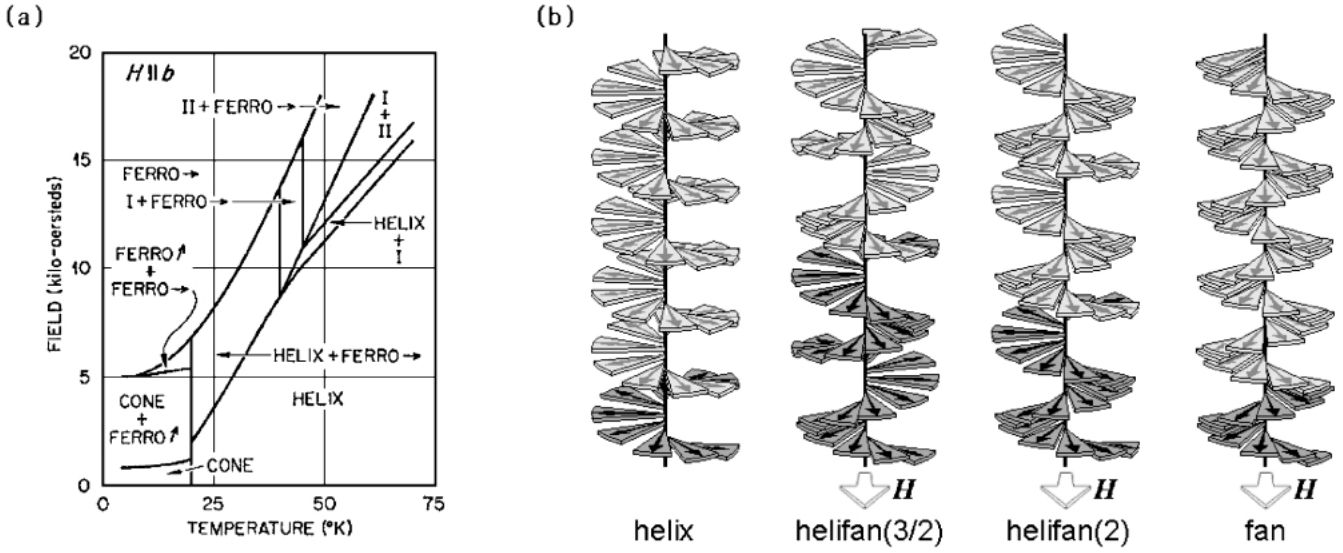

Fig. 1. (a) Schematic *H–T* phase diagram for single-crystal holmium with a magnetic field applied along the *b*-axis. From Koehler *et al.*[4] (b) The helix, helifan(3/2), helifan(2) and fan structure in Ho at 80 K. The moments lie in planes normal to the *c*-axis and their relative orientations are indicated by arrows. A magnetic field is applied along the *b*-axis in the basal plane to the helifans and fan. The shaded parts of the illustrations indicate the respective magnetic unit cells.

*Present address: Japan Synchrotron Radiation Research Institute, Kouto 1-1-1, Mikazuki, Sayo, Hyogo 679-5198.

decades. In recent years, interest in the extra phase has resurged because of its novelty in the magnetic structure. Based on the self-consistent mean field calculation, Jensen and Mackintosh proposed a new type of magnetic structure, a helifan,[16–18] which is an intermediate structure between the helix and the fan. Schematic views of the helifans are shown in Fig. 1(b), together with the helix and fan structures. The existence of the helifan structure was actually confirmed by a neutron diffraction experiment.[12] Not only the magnetic structures of holmium[8,16,19] but also those of the other rare earth metal[20,21] are remarkably well reproduced by the self-consistent mean field calculation.

In rare earth metals, crystal lattices are strongly influenced[6–8,22–24] by a magnetic structure through the strong magnetoelastic coupling and a giant magnetostriction[25,26] is observed in low temperatures. The temperature dependence of the lattice parameters was explained in terms of an exchange magnetostriction.[26–28] Recently, X-ray diffraction experiments on rare earth metals[24,29,30] have been performed to study both the change in the lattice parameter and the appearance of the lattice modulations accompanying magnetic structural changes. From these X-ray diffraction experiments, we could well examine the magnetic structures through the magnetoelastic effect.[24,29,30] In holmium, magnetic structural phase transitions have been observed as discontinuous and continuous changes in the c-lattice parameter[1] and the lattice modulation has been found in the distorted helix and helifan phases.[2] This study was motivated, in part, by interest in the helifan, which is not understood entirely. Therefore, we attempt to make a detailed discussion on the helifan with assistance of the self-consistent mean field calculation which reproduces the magnetic structures of heavy rare earth metals very well, though the magnetic structure was not directly observed in this study.

2. Experiments

2.1 Experimental details

X-ray diffraction measurements were performed on a holmium single crystal sample. The Cu Kα radiation (40 kV, 300 mA) from a conventional rotating anode source was used as an incident beam. A vertically bent pyrolytic graphite(002) monochrometer was used to focus the beam on a sample position. In the c-lattice parameter measurements, a flat germanium(111) was used as an analyzer and slits were tightly collimated in order to eliminate the reflection of Kα_2 radiation. A typical diffractometer resolution along the longitudinal direction was approximately 0.008 Å^{-1}. For measurements of satellite reflections, a flat pyrolytic graphite(002) analyzer with loose collimation was used to detect weak intensity of satellites. The surface of the sample was normal to the c-axis, and the measurements were made along the $\langle 00L \rangle$ direction. A magnetic field up to 8 T was applied along the easy direction of holmium, b-axis, by a split solenoids type superconducting magnet which is installed on a large goniometer head.

2.2 c-lattice parameter

As a magnetic field increased below T_N, the c-lattice parameter exhibited several discontinuous changes. Figure 2 shows diffraction patterns of the (006) Bragg reflection along the $\langle 00L \rangle$ direction in various magnetic fields at 60 K. As seen in Fig. 1(a), the helix and ferromagnetic structures are singly formed at 0.0 T and 6.0 T, respectively. The line profiles of the (006) Bragg reflection at those magnetic fields have a squared Lorentzian shape. By fitting the line profiles with sums of squared Lorentzians centered at different wave numbers, the c-lattice parameter was found to change discontinuously three times in an increasing field process at this temperature. The discontinuous changes in the c-lattice parameter coincide with the magnetic phase transitions shown in Fig. 1(a). At this temperature, helix, helifan, fan and ferromagnetic structures appear in sequence from low magnetic field. Since the magnetic structures exhibit a different degree of magnetostriction, we could distinguish one magnetic structure from others using the c-lattice parameter. With decreasing magnetic field, the peak position was found to shift continuously from the helifan to the helix as seen in Fig. 2(b). This behavior cannot be explained with a picture of coexistence of two competing phases. Further, an absence of the broadening of a line profile indicates uniformity of magnetostriction on this transition.

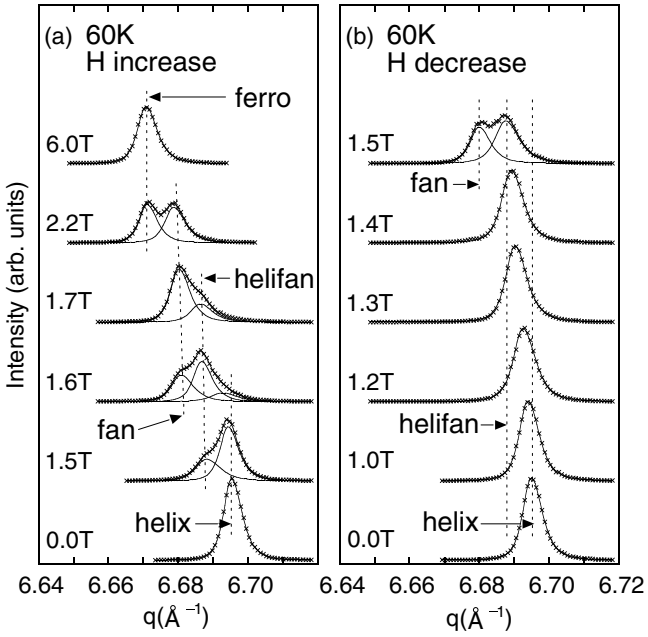

Fig. 2. Diffraction patterns of the (006) Bragg reflection at 60 K in various magnetic fields. The solid lines represent the result of peak separation by fitting. The vertical broken lines indicate the peak position of the diffraction lines corresponding to the helix, helifan, fan and ferromagnetic structures. (a) Measurements with increasing magnetic field. (b) Measurements with decreasing magnetic field.

Figures 3(a)–3(d) show the magnetic field dependence of the c-lattice parameter at various temperatures, which are determined from the (006) Bragg reflection. Open and closed circles are the values obtained with increasing and decreasing magnetic field, respectively. In these figures, c_0 is the "non-magnetic" c-lattice parameter obtained by extrapolation from the high temperature paramagnetic region. The solid lines in the figures represent the numerically calculated magnetostriction for the magnetic structures which will be shown below. Identification of magnetic structures were again made according to Fig. 1(a). Figure 3(a) shows the magnetic field dependence of the c-lattice parameter at 40 K.

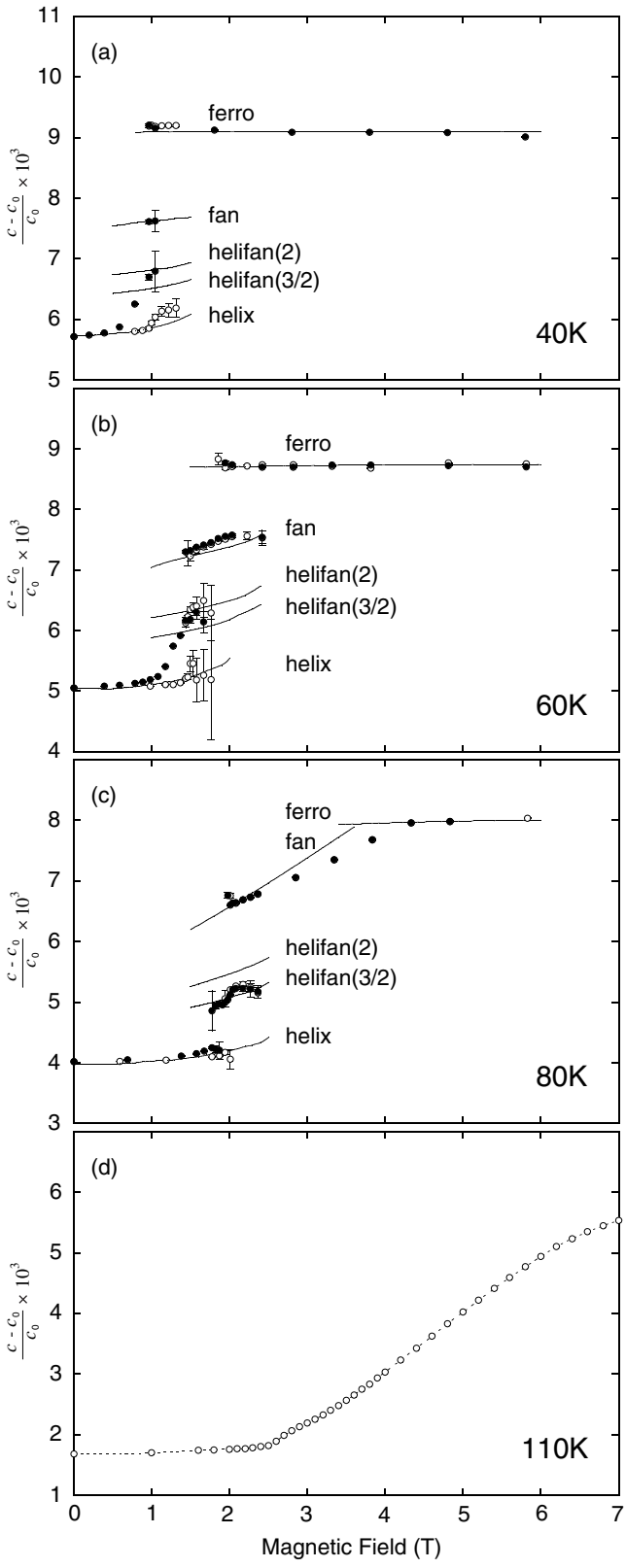

Fig. 3. The magnetic field dependence of the c-lattice parameter at (a) 40 K, (b) 60 K, (c) 80 K and (d) 100 K. The solid lines represent the calculated values for the magnetic structures. The broken line for 100 K is the guide for eye. Open and filled circles are the results obtained with increasing and decreasing magnetic field, respectively.

The c-lattice parameter exhibits a discontinuous change around 1.0 T with increasing magnetic field. This corresponds to a magnetic phase transition from the helix to ferromagnet. With decreasing magnetic field, the c-lattice parameter changes differently from the increasing field process below the transition field. The magnetostriction which does not correspond to that of the helix and ferromagnet indicates the appearance of the other magnetic structure. The large hysteresis for a magnetic field was found also in a magnetoresistance measurement.[15] The magnetic field dependence of the c-lattice parameter at 60 K is summarized in Fig. 3(b). Four different magnetic structures appeared at this temperature as mentioned above. In an increasing field process, all the transitions, helix to helifan, helifan to fan and fan to ferromagnet, accompany a discontinuous change in the c-lattice parameter. The helifan to helix transition was found to be continuous in a decreasing field process, which is completely different from the increasing field process. At 80 K, no difference was found between increasing and decreasing field processes as seen in Fig. 3(c). With increasing magnetic field, two transitions, helix to helifan and helifan to fan, occur successively around 2.0 T. The fan to ferromagnet transition is no longer discontinuous at this high temperature range, because the anisotropy in the basal c-plane is supposed to be negligible.[13,26] Figure 3(d) shows the magnetic field dependence of the c-lattice parameter at 110 K. The magnetic field up to 7 T seems to be insufficient for the system to reach the ferromagnetic structure. Although a magnetic structure changes from the helix to fan around 2.4 T, no discontinuous change in the c-lattice parameter was detected. However, from the result of the self-consistent mean field calculation which will be discussed below, this transition is expected to be discontinuous in magnetization and magnetostriction because of the occurrence of spin flip. This unexpected behavior just below T_N was reported also in Dy.[29] This may be the limit of a mean field calculation which does not take fluctuations into account.

2.3 *Lattice modulations*

The lattice modulation is expected for a magnetic structure in which there are several non-equivalent sublattices. Therefore, no lattice modulation occurs in the helix phase with zero magnetic field and in the ferromagnetic phase, because the turn angle between the moments on successive planes is constant through atomic layers. In other magnetic phases, however, we expected to observe the satellite reflection caused by the lattice modulation.

Figure 4 shows diffraction patterns along the $\langle 00L \rangle$ direction at 80 K in a field range for the distorted helix phase. A satellite reflection appears at $(0, 0, 6 - \tau_{\mathrm{lat}})$ position where τ_{lat} is the same as the fundamental wave number of the magnetic modulation. Double peaks in the diffraction patterns are caused by two incident X-ray beams of $K\alpha_1$ and $K\alpha_2$ from the Cu target. Intensity of the satellite reflection increases with increasing magnetic field, but it decreases abruptly around 1.8 T, because the magnetic structural change to the helifan(3/2) occurs.

Figure 5 shows diffraction patterns along the $\langle 00L \rangle$ direction at 80 K in a field range for the helifan phase. The solid line represents the result of fitting with a squared Lorentzian function. With increasing magnetic field, two broad satellites having different wave numbers appear at the magnetic field of 2.0 T as shown in Fig. 5(a). The broadening

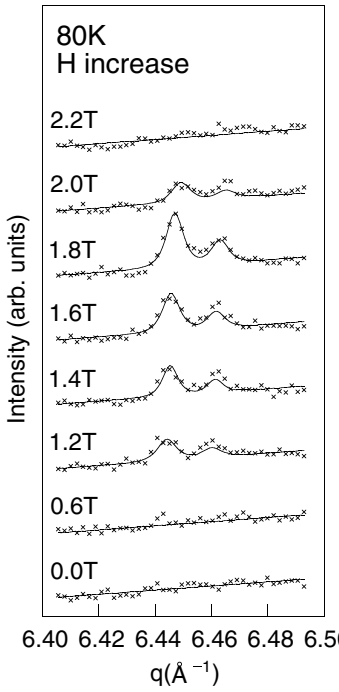

Fig. 4. Diffraction patterns along the $\langle 00L \rangle$ direction near the (006) Bragg reflection at 80 K in various magnetic fields. Measurements were made with increasing magnetic field.

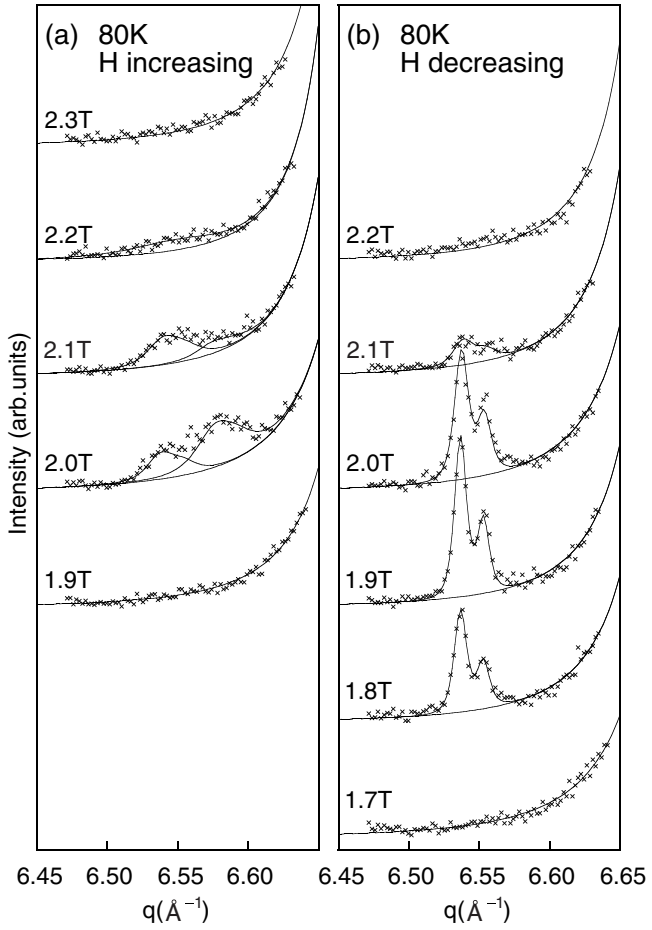

Fig. 5. Diffraction patterns along the $\langle 00L \rangle$ direction near the (006) Bragg reflection at 80 K in various magnetic fields. (a) Measurements with increasing magnetic field. (b) Measurements with decreasing magnetic field.

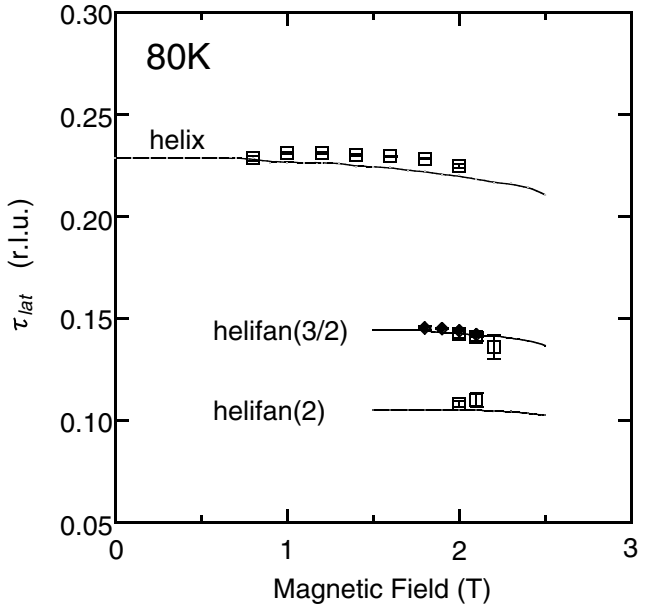

Fig. 6. The magnetic field dependence of the reduced wave number τ_{lat} determined from the positions of the satellite reflections. The solid lines represent the calculated τ_{lat} of the magnetic structures.

of the line profile of the satellite indicates that domains of the helifan phase are small. The satellite reflection disappears above 2.2 T and no other satellite is observed above this magnetic field. With decreasing magnetic field, the satellite reflection appears in a range between 2.1 T and 1.8 T, as shown in Fig. 5(b). In contrast to the increasing field process, only one satellite was observed and the width of the line profile was within the resolution of the diffractometer. Double peaks of the diffraction patterns in Fig. 5(b) are again caused by $K\alpha_1$ and $K\alpha_2$.

The magnetic field dependence of the lattice modulation wave number at 80 K is summarized in Fig. 6. Open and filled symbols are the experimental data obtained with increasing and decreasing magnetic field, respectively. The solid lines in the figure represent the result of the self-consistent mean field calculation described below. The two helifans observed in an increasing field process are the helifan(3/2) and helifan(2), and only the helifan(3/2) was observed in a decreasing field process.

The amplitude of the lattice modulation can be estimated from the intensity ratio of the satellite to the (006) Bragg reflection. Figure 7 shows the amplitude of the lattice modulation for the distorted helix and helifan(3/2) magnetic structures observed at 80 K. The solid lines in the figure are the values expected from the model described below. The amplitude shown in Fig. 7 is obtained from a decreasing field process in which the helifan(3/2) appears as a single phase. When there is no coexisting phase, an estimation of the amplitude becomes straightforward. Intensity of the satellite reflection for the helifan structures is one order of magnitude stronger than that for the distorted helix, but no satellite could be detected in the fan phase.

Measurements of the satellite have been extended to various temperatures between 30 K and 110 K. The wave number of all the satellites observed in an increasing field process at several temperatures are summarized in Fig. 8(a). The solid line in the figure is the temperature dependence of

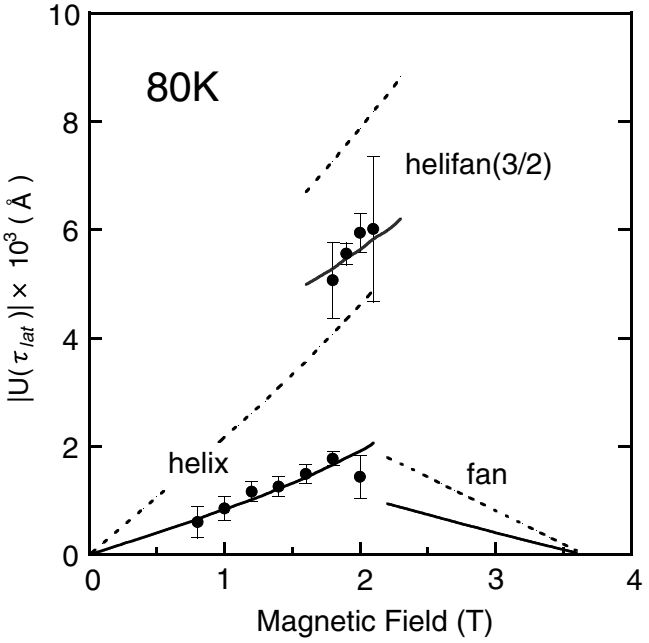

Fig. 7. The magnetic field dependence of the lattice modulation amplitude at 80 K. The solid lines are the value expected from the model.

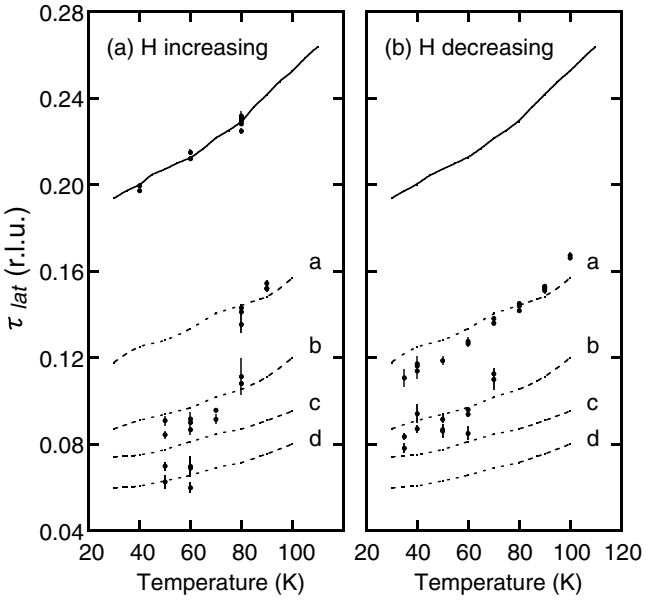

Fig. 8. The temperature dependence of the reduced wave number τ_{lat} determined from the positions of the satellite reflections. A solid line represents the reduced wave number of the helical magnetic structure in zero field (quoted from ref. 4). Broken lines (a, b, c and d) represent the calculated τ_{lat} of the helifans (3/2, 2, 5/2 and 3, respectively). (a) Measurements with increasing magnetic field. (b) Measurements with decreasing magnetic field.

the wave number of the helical magnetic structure determined from a neutron diffraction experiment in a zero magnetic field,[4] and the wave number of the lattice modulation which is induced by the distorted helix agrees with that of the magnetic modulation very well. The broken lines in the figure represent the temperature dependence of the lattice modulation wave number for various helifan structures reproduced by the self-consistent mean field calculation. In an increasing field process, one or two broad

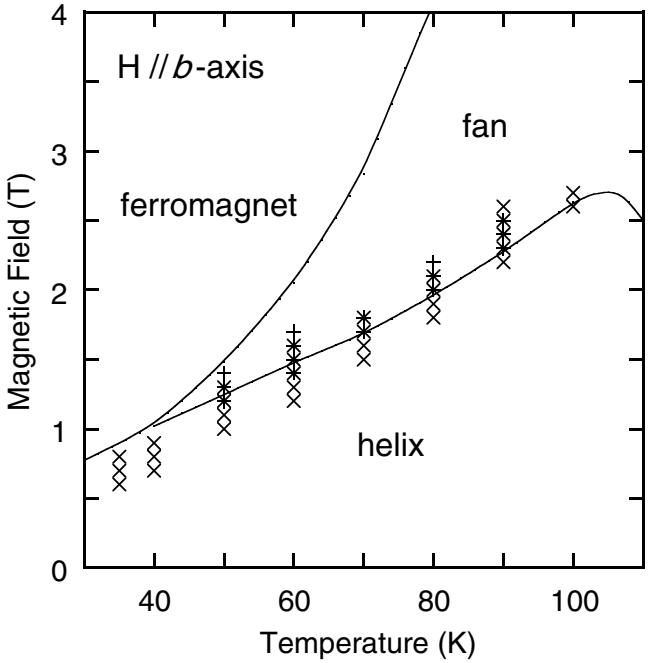

Fig. 9. The H–T magnetic phase diagram of holmium for the magnetic field along the b-axis. The detection of the satellite reflection in increasing and decreasing processes are represented as (+) and (×) symbols, respectively.

satellites were observed in a temperature range between 50 K and 90 K. From the wave number of the satellite, they are considered as the helifan(3/2) and/or helifan(2) and/or helifan(3). The reason for the appearance of the helifan(3), not helifan(5/2), will be discussed in the next section. On the other hand, only the helifan(3/2) and helifan(2) were observed in a decreasing field process as seen in Fig. 8(b). The shape, peak intensity and number of satellites are different between in increasing and decreasing field processes. Well-defined sharp satellites as seen in Fig. 5(b) were detected at a temperature range between 70 K and 100 K in a decreasing field process, while most satellites were found to be broad.

The region for observing satellites caused by the helifans in the H–T magnetic phase diagram is shown in Fig. 9. In this figure, (+) and (×) are the symbols for detecting the satellite reflections in an increasing and decreasing field process, respectively. Observing the satellite reflection is an explicit way to determine the range of the helifan in the magnetic phase diagram. On the other hand, the appearance of the helifan phase can be detected also by observing the Bragg reflection, but an elaborate analysis is necessary to separate the Bragg reflection of the helifan structure among coexisting other structures as shown in Fig. 2(a). The observations of the Bragg and satellite reflections have given a consistent result on the magnetic phase diagram.

3. Analysis and Discussion

Information about the magnetic structures is indispensable to describe the behavior of the lattice. The self-consistent mean field method developed by Jensen and Mackintosh[16–18] was employed in reproducing various magnetic structures. The Hamiltonian for the k-th ion (layer) is written as

Table I. The parameters used in the calculations (all values are in meV). The remaining parameters are follows: $B_2^0 = 0.0240$, $B_4^0 = 0$, $B_6^0 = -9.56 \times 10^{-7}$, $B_6^6 = 9.21 \times 10^{-6}$.

T (K)	$\mathcal{J}_0$	$\mathcal{J}_1$	$\mathcal{J}_2$	$\mathcal{J}_3$	$\mathcal{J}_4$	$\mathcal{J}_5$	$\mathcal{J}_6$
40	0.19585	0.09613	0.00621	−0.02285	−0.00512	0.00442	−0.00310
60	0.21908	0.10670	0.00993	−0.03300	−0.00356	0.00631	−0.00373
80	0.23697	0.11000	0.01000	−0.04020	0.00150	0.00280	−0.00230

$$\mathcal{H}_k^{MF} = \sum_{lm} B_l^m O_l^m(\boldsymbol{J}_k) - \sum_n \mathcal{J}_n \langle \boldsymbol{J}_{k+n} \rangle \cdot \boldsymbol{J}_k + \frac{1}{2} \sum_n \mathcal{J}_n \langle \boldsymbol{J}_{k+n} \rangle \cdot \langle \boldsymbol{J}_k \rangle - g\mu_B \boldsymbol{H} \cdot \boldsymbol{J}_k. \quad (1)$$

The first term is the crystal-field contribution represented by the Stevens operators $O_l^m(\boldsymbol{J}_k)$ and the crystal-field parameters B_l^m. The inter-planer exchange coupling parameters $\mathcal{J}_n$ are extracted from $\mathcal{J}(q) - \mathcal{J}(0)$ which depends on temperature.[19,31] $\mathcal{J}_3$ was slightly modified in order to reproduce the experimentally obtained wave number of the helix in a zero magnetic field. The isothermal magnetization curve was fitted with a variable parameter $\mathcal{J}_0$. The 6-th order crystal field anisotropy was neglected[26] in calculations for temperatures of 80 K and above. All the parameters used in the calculations are given in Table I. The magnetic structures are assumed commensurable to the crystal lattice with a cycle about 100–150 atomic layers. A distribution of thermal expectation values $\langle \boldsymbol{J}_k \rangle$ is calculated using the self-consistent mean field method and the stable magnetic structure in a given magnetic field is determined so as to have the minimum free energy among various magnetic structures.

The calculated isothermal magnetization curves are shown as solid lines in Fig. 10. In this figure, open and filled symbols are the experimental data obtained with increasing and decreasing magnetic field, respectively. According to the calculations, the helifan(3/2) is stable only in a narrow field range at temperatures between 40 K and 100 K. All the phase transitions are accompanied by an abrupt jump in magnetization except the fan to ferromagnet transition at 80 K. At this transition from the fan to ferromagnet, free energy changes smoothly with magnetic field, although the other transitions exhibit kinks on the free energy curve. Taking into account the coexistence of phases in the process of the first order phase transition, the step like behavior of calculated magnetization will become smooth like the observations. The transition fields are estimated slightly higher for 40 K and lower for 80 K, but the magnetization curves can be explained by using the metastable region of the coexisting phases. Therefore, the results of the calculations are considered to be in good agreement with the experimental data, which indicates the magnetic structure under magnetic field can be well reproduced by the self-consistent mean field method.

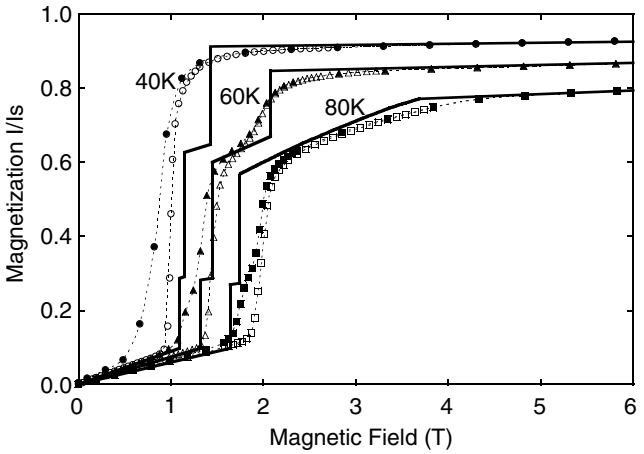

Fig. 10. Magnetization curves at various temperatures. The solid lines are the calculated results for the stable phases. Open and closed symbols are the experimental data obtained with increasing and decreasing magnetic field, respectively.

The model of the exchange magnetostriction is based on the idea that the exchange interaction depends on the distance between magnetic moments.[1,26–29] A lattice modulation which is induced by a magnetic structure was also explained with the same idea.[24] Here, the model of the exchange magnetostriction is extended to include the lattice modulation. The concurrent treatment of both the magnetoelastic effects on the lattice parameter and the lattice modulation was proposed also for Er[30,33] and $DyZn_2$.[32] The position of the k-th c-plane can be written as

$$r_k = \frac{1}{2} k c_0 (1 + \varepsilon) + u_k, \quad (2)$$

where c_0 is the c-lattice parameter in the absence of the magnetic interaction, $\varepsilon = \frac{c - c_0}{c_0}$ represents the strain caused by the magnetic interaction and u_k denotes a small displacement which depends on sites. The elastic energy E_e of the magnetic unit cell is given by

$$E_e = \frac{N\varepsilon^2 c_0^2}{16\pi^2} \left. \frac{\partial^2 \Phi(\zeta)}{\partial \zeta^2} \right|_{\zeta=0} + \frac{1}{2} \sum_{n=-\infty}^{+\infty} \sum_{k=0}^{N-1} \Phi_n u_{k+n} u_k, \quad (3)$$

where Φ_n is the inter-planer force constant, N is the number of planes included in the magnetic unit cell and ζ is the reduced wave number in the $\langle 00L \rangle$ direction. We next consider the modification of the magnetic energy by a magnetoelastic coupling. Since the displacement u_k is considered to be small, B_0^2 and $\mathcal{J}_n$ can be expanded in a Taylor series. Neglecting the second and higher order terms, the magnetoelastic energy E_{me} of the magnetic unit cell is written as follows:

$$E_{me} = \frac{D}{2} \sum_{k=0}^{N-1} [c_0 \varepsilon + u_{k+1} - u_{k-1}] \langle O_2^0(\boldsymbol{J}_k) \rangle - \frac{1}{2} \sum_{n=-\infty}^{+\infty} \sum_{k=0}^{N-1} K_n \left[\frac{n c_0}{2} \varepsilon + u_{k+n} - u_k \right] \langle \boldsymbol{J}_{k+n} \rangle \cdot \langle \boldsymbol{J}_k \rangle, \quad (4)$$

where differential coefficients are symbolized as $D = B_2^{0\prime}(\frac{c_0}{2})$ and $K_n = \mathcal{J}'(\frac{nc_0}{2})$.

The equilibrium value of ε minimizes the total energy E. Differentiating E with respect to ε, we obtain the expression for the equilibrium strain

$$\left(\frac{c_0}{4\pi^2}\frac{\partial^2\Phi(\zeta)}{\partial\zeta^2}\bigg|_{\zeta=0}\right)\varepsilon = -D\left[\frac{1}{N}\sum_{k=0}^{N-1}\langle O_2^0(\boldsymbol{J}_k)\rangle\right] + \sum_{n=1}^{+\infty} nK_n\left[\frac{1}{N}\sum_{k=0}^{N-1}\langle \boldsymbol{J}_{k+n}\rangle\cdot\langle \boldsymbol{J}_k\rangle\right]. \tag{5}$$

Similarly, differentiating E with respect to u_k, the expression for the equilibrium displacement is written as

$$\sum_{n=-\infty}^{+\infty}\Phi_n u_{k+n} = \frac{D}{2}\left[\langle O_2^0(\boldsymbol{J}_{k+1})\rangle - \langle O_2^0(\boldsymbol{J}_{k-1})\rangle\right] - \sum_{n=-\infty}^{+\infty} K_n\langle \boldsymbol{J}_{k+n}\rangle\cdot\langle \boldsymbol{J}_k\rangle. \tag{6}$$

We assume u_k is expressed as

$$u_k = \sum_l U(l\zeta_m)e^{i\pi\zeta_m lk}, \tag{7}$$

where ζ_m is the wave number of a magnetic structure and l is determined by cyclic boundary conditions to be $l\zeta_m$ in the Brillouin zone. The thermal expectation values $\langle O_2^0(\boldsymbol{J}_k)\rangle$ and $\langle \boldsymbol{J}_k\rangle$ are expanded in a Fourier series as follows:

$$\langle O_2^0(\boldsymbol{J}_k)\rangle = \sum_h O(h\zeta_m)e^{i\pi\zeta_m hk}, \tag{8a}$$

$$\langle \boldsymbol{J}_k\rangle = \sum_m \boldsymbol{J}(m\zeta_m)e^{i\pi\zeta_m mk}. \tag{8b}$$

Substituting eqs. (7), (8a), (8b) into eq. (6) leads to the following expression

$$\Phi(l\zeta_m)U(l\zeta_m) = iD\sin\pi l\zeta_m O(l\zeta_m) - \sum_{m=0}^{l} K(m\zeta_m)\boldsymbol{J}(m\zeta_m)\cdot\boldsymbol{J}((l-m)\zeta_m), \tag{9}$$

where $\Phi(\zeta)-\Phi(0) = 2\sum_{n=1}^{+\infty}\Phi_n[\cos(\pi n\zeta)-1]$ and $K(\zeta) = 2i\sum_{n=1}^{+\infty}K_n\sin(\pi n\zeta)$.

We now obtain the final forms of the equilibrium strain and displacement. Concerning the expectation values $\langle O_2^0(\boldsymbol{J}_k)\rangle$ and $\langle \boldsymbol{J}_k\rangle$, the results of the numerical calculations are used in an analysis of the experimental data. The magnetoelastic coupling constants are obtained by fitting the results of the magnetic field dependence of the c-lattice parameter with eq. (5). The amplitude of the lattice modulation can be estimated from eq. (9) by using the same magnetoelastic coupling constants. The c-lattice parameter and lattice modulation should be concurrently explained by using the same magnetoelastic coupling constants.

The results of the fitting for the c-lattice parameter are shown as solid lines in Fig. 3. All the magnetoelastic coupling constants determined by the fitting are tabulated in Table II. The inter planer force constants Φ_n in eq. (5) are deduced from the phonon dispersion relation of holmium at room temperature,[34] where Φ_1 and Φ_2 are -2000 and -21.59 in units of meV/Å^2, respectively. The temperature dependence of the inter planer force constants is neglected in the present analysis. Concerning the helifan to helix transition in a decreasing field process at 40 K and 60 K, the continuous change in the c-lattice parameter could not be reproduced with the calculated magnetic structures as seen in Figs. 3(a) and 3(b). Since no satellite reflection was observed during the transition, it is plausible that magnetic moments flip randomly not to have long-range correlation but to be proportional to magnetic field. This successive change of the spin configuration is not taken into account in the present model calculation of a magnetic structure.

Table II. The fitting parameters (all values are in meV/Å).

T(K)	D	K_1	K_2	K_3
40	−2.8768	4.8225	−2.2790	0.64907
60	−4.1365	6.1482	−2.5605	0.71568
80	−4.7266	5.5324	−1.4049	0.35995

We next consider the order of the fitting parameters required, concerning the magnetoelastic coupling constants D and K_n. In the previous paper,[1] we reported that the magnetic field dependence of the c-lattice parameter can be explained by introducing three parameters D, K_1 and K_2. However, the amplitude of the lattice modulation cannot be well reproduced with the obtained values of D, K_1 and K_2. The dotted lines in Fig. 7 are the calculated amplitude of the lattice modulation and an agreement with the experimental results is unsatisfactory. A remarkable improvement in reproducing the amplitude of the lattice modulation is attained by introducing K_3. The solid lines in Fig. 7, which agree with the experimental results very well, are the result of fitting with K_3. Consequently, we need to include at least four magnetoelastic coupling constants D, K_1, K_2 and K_3 in the fitting. The c-lattice parameter and lattice modulation were found to be concurrently explained by using the same magnetoelastic coupling constants, indicating that the influence of a magnetic structure on a crystal lattice is satisfactorily described by the exchange magnetostriction model which is extended to include the lattice modulation.

The lattice modulation is expected to be induced also in the fan phase. However, no appreciable satellite reflection could be observed despite repeated surveys in the fan phase. According to the model, the amplitude of the lattice modulation for the fan structure is estimated to be smaller than that of the distorted helix at 1.2 T shown in Fig. 4. It is supposed that such a weak satellite reflection can scarcely be observed by using a conventional rotating anode source X-ray as in the present experiment.

The present model could explain the experimental result that the helifans exhibit intermediate magnetostriction between those of the helix and fan. However, it is difficult to distinguish a particular helifan among helifans by a slight difference in the c-lattice parameter. Observing the satellite reflection provides another way to identify a magnetic structure. The wave number of the lattice modulation is peculiar to respective magnetic structures and exhibits the explicit difference between each other.

The magnetic field dependence of the wave numbers of the lattice modulations at 80 K is shown in Fig. 6. The agreement between the experiment and the calculation by the self-consistent mean field method is fairly good. The observed helifans can be clearly identified as the helifan(3/2)

and helifan(2). On the other hand, more detailed consideration has to be made with regard to the temperature dependence of the wave number of the lattice modulations shown in Fig. 8. Most lattice modulations can be identified as those induced by the helifan(3/2) and helifan(2). However, the helifan(5/2) and helifan(3)[16] can be a possible magnetic structure which would corresponds to the lattice modulation with the smallest wave numbers shown in Fig. 8(a). As mentioned by Jensen and Mackintosh,[16] it is supposed that the energy barrier for generating the helifan(5/2) in an increasing field process would be high because this structure is a type of the helifan(half integer). This is also supposed to be the reason for the absence of the helifan(3/2) in an increasing field process at lower temperature. Therefore, the helifan(5/2) would be excluded from possible magnetic structures for the lattice modulation. One can consider two types of helifan(3)[16] written as $(+\ +\ +\ -\ +\ -)$ or $(+\ +\ +\ +\ +\ -)$. The former type has smaller magnetization than those of the latter and the helifan(2). Since the helifan under consideration was observed at lower fields than those for helifan(2), the former type of helifan(3) is chosen as the magnetic structure which induces the lattice modulation with the smallest wave numbers.

4. Conclusion

In the present study we have performed X-ray diffraction studies on holmium single crystal. Application of a magnetic field along the *b*-axis causes abrupt changes in the *c*-lattice parameter followed by magnetic phase transitions. This magnetoelastic behavior provides a way of probing the magnetic structures of the system by means of X-ray diffraction. We have exposed the existence of the lattice modulation by observing the satellite reflection around the Bragg reflection. The helifan magnetic structure was precisely studied regarding an appearance region and a period of the structure. The region for the helifans has been confirmed on the *H–T* phase diagram. A numerical calculation by the self-consistent mean field method[16] was performed to reproduce magnetic structures. A model for the magnetoelastic effect, which is based on the exchange magnetostriction,[28] was extended to include the lattice modulation. We have shown concurrent explanation for the magnetoelastic effects on the *c*-lattice parameter and for the lattice modulation. Extensive measurements by using a synchrotron X-ray are needed to detect the higher order satellite reflection, which will play a significant role in determination of the magnetoelastic coupling constants.

Acknowledgments

The author would like to thank Y. Shinoda for growing a single crystal of holmium, Professor K. Tajima and Professor N. Wakabayashi for valuable discussions and Dr. S. Shimomura, Dr. G. Masada, Messrs. Y. Kida and S. Shinjo for their assistance in X-ray measurements. This work was partly supported by a Grant-in-Aid for Science Research from the Ministry of Education, Culture, Sports, Science and Technology, Japan.

1) H. Ohsumi, K. Tajima, N. Wakabayashi, Y. Shinoda, K. Kamishima and T. Goto: J. Phys. Soc. Jpn. **66** (1997) 1896.
2) H. Ohsumi and K. Tajima: J. Phys. Soc. Jpn. **67** (1998) 1883.
3) W. C. Koehler, J. W. Cable, M. K. Wilkinson and E. O. Wollan: Phys. Rev. **151** (1966) 414.
4) W. C. Koehler, J. W. Cable, H. R. Child, M. K. Wilkinson and E. O. Wollan: Phys. Rev. **158** (1967) 450.
5) M. Pechan and C. Stassis: J. Appl. Phys. **55** (1984) 1900.
6) D. Gibbs, D. E. Moncton, K. L. D'Amico, J. Bohr and B. Grier: Phys. Rev. Lett. **55** (1985) 234.
7) J. Bohr, D. Gibbs, D. E. Moncton and K. L. D'Amico: Physica A **140** (1986) 349.
8) J. Bohr, D. Gibbs, J. D. Axe, D. E. Moncton, K. L. D'Amico, C. F. Majkrzak, J. Kwo, M. Hong, C. L. Chien and J. Jensen: Physica B **159** (1989) 93.
9) R. A. Cowley and S. Bates: J. Phys. C **21** (1988) 4113.
10) S. Bates, C. Patterson, G. J. McIntyre, S. B. Palmer, A. Mayer, R. A. Cowley and R. Melville: J. Phys. C **21** (1988) 4125.
11) G. Helgesen, J. P. Hill, T. R. Thurston, D. Gibbs, J. Kwo and M. Hong: Phys. Rev. B **50** (1994) 2990.
12) D. A. Jehan, D. F. McMorrow, R. A. Cowley and G. J. McIntyre: J. Magn. & Magn. Mater. **104–107** (1992) 1523.
13) Y. Kitano and T. Nagamiya: Prog. Theor. Phys. **31** (1964) 1.
14) D. L. Strandburg, S. Legvold and F. H. Spedding: Phys. Rev. **127** (1962) 2046.
15) M. Akhavan and H. A. Blackstead: Phys. Rev. B **13** (1976) 1209.
16) J. Jensen and A. R. Mackintosh: Phys. Rev. Lett. **64** (1990) 2699.
17) J. Jensen and A. R. Mackintosh: J. Magn. & Magn. Mater. **104–107** (1992) 1481.
18) A. R. Mackintosh and J. Jensen: Physica B **180&181** (1992) 1.
19) C. C. Larsen, J. Jensen and A. R. Mackintosh: Phys. Rev. Lett. **59** (1987) 712.
20) R. A. Cowley and J. Jensen: J. Phys.: Condens. Matter **4** (1992) 9673.
21) N. Wakabayashi, J. W. Cable and J. L. Robertson: Physica B **241–243** (1998) 517.
22) D. Gibbs, J. Bohr, J. D. Axe, D. E. Moncton and K. L. D'Amico: Phys. Rev. B **34** (1986) 8182.
23) J. Bohr, D. Gibbs and K. Huang: Phys. Rev. B **42** (1990) 4322.
24) K. Iwasa, N. Wakabayashi, T. Takabatake, H. Fujii and T. Shigeoka: J. Phys. Soc. Jpn. **63** (1994) 127.
25) S. Legvold, J. Alstad and J. Rhyne: Phys. Rev. Lett. **10** (1963) 509.
26) J. J. Rhyne, S. Legvold and E. T. Rodine: Phys. Rev. **154** (1967) 266.
27) F. J. Darnell: Phys. Rev. **130** (1963) 1825.
28) E. W. Lee: Proc. Phys. Soc. **84** (1964) 693.
29) Y. Kida, K. Tajima, Y. Shinoda, K. Hayashi and H. Ohsumi: J. Phys. Soc. Jpn. **68** (1999) 650.
30) G. Masada and K. Tajima: J. Phys. Soc. Jpn. **68** (1999) 2414.
31) J. Jensen and A. R. Mackintosh: *Rare Earth Magnetism* (Clarendon Press, Oxford, 1991) p. 115.
32) Y. Wakabayashi, N. Wakabayashi and T. Kitai: J. Phys. Soc. Jpn. **67** (1998) 3901.
33) K. Tajima, H. Ohsumi and G. Masada: Mater. Trans. JIM **41** (2000) 1040.
34) R. M. Nicklow, N. Wakabayashi and P. R. Vijayaraghavan: Phys. Rev. B **3** (1971) 1229.